



Experimental Investigation of the Effect of Louver Scheme Internal Bend and Exit Shape on the Film Cooling Performance over a Flat Plate

O. Hassan

Department of Mechanical Engineering, Assiut
University, Assiut, Egypt, 71516

T. Elnady

Department of Mechanical Engineering,
Egyptian Armed Forces

ABSTRACT

This paper presents experimental investigations of the effects of the presence of an internal 90° bend and the design of the scheme exit on the film cooling performance of the louver scheme over a flat plate using the transient Thermo-chromic Liquid Crystal (TLC) technique. The Louver scheme is a shaped scheme with an internal 90° bend, circular hole followed by a horizontal slot, which adds the impingement cooling benefits to the enhanced film cooling performance of shaped schemes. The louver film cooling scheme was manufactured in the present study with two different exit designs. The first is characterized with straight interfaces between the scheme and the test surface and the second has curved interface lines. Meanwhile, a third scheme was manufactured with the same exit shaped of the louver with curved interface lines, but without the internal 90° bend. The film cooling performance of the proposed designs was investigated at three different blowing ratios, 0.5, 1.0 and 1.5, a density ratio of 0.93, a Reynolds Number of 1.24E+5, based on the free stream velocity and the main duct hydraulic diameter, and a turbulence intensity of 8.5. The blowing ratio is calculated based on the base diameter of the louver scheme and the same coolant amount is supplied to all cases. The investigations showed that the scheme exit design has a significant effect on the resulting effectiveness as it affects the interaction nature between the main and the secondary streams. This was clear during the investigations through the enhanced effectiveness performance downstream the louver scheme with curved exit design, compared to the louver with straight exit. Also, adding a 90° internal bend to the shaped scheme design for impingement cooling purposes does not have a contribution on the scheme film cooling performance. Changing the film cooling scheme design did not affect the resulting heat transfer coefficient distribution significantly. This was attributed to the small change in the supplied coolant mass due to using the scheme base diameter for blowing ratio calculations.

Key Words; Gas turbines, Film cooling, Louver Scheme, Shaped Scheme, Effectiveness, Heat Transfer Coefficient

1. INTRODUCTION

During the past few decades, numerous research works have been conducted in the area of gas turbine engines cooling to introduce better cooling techniques that can cope with the increasing demand of power generation. Combustion gases enter the turbine at very high temperatures reaching 1900K, so efficient cooling techniques are essential to protect the engine components. Internal passage cooling, impingement cooling on the inner surfaces, and film cooling are the typical cooling techniques being used nowadays. Among all of these cooling techniques, film cooling is the most important one. Many parameters affect the performance of film cooling in terms of effectiveness and Heat Transfer Coefficient (HTC) values. The injection scheme geometry and the blowing ratio were found to have significant effect on the film cooling performance. Shaped schemes showed enhanced film cooling performance compared to normal circular and compound circular schemes.

The early design of film cooling schemes was in the form of continuous slots. The inclination angle of the injection scheme is of special importance because it highly affects the performance of the scheme. Zero inclination angle, otherwise known as tangential injection, was shown to be the best scenario by Goldstein et al. [1], Hartnett et al. [2], Wiegardt [3], and many others. Numerous experimental investigations had been conducted to investigate the effect of different geometrical and flow parameters on the film cooling performance of slot schemes with tangential injection. Researchers then switched to discrete-holes tangential injection schemes, in order to sustain reasonable material strength. To enhance the performance of discrete holes tangential injection schemes, Folyan and Whitelaw [4] proposed a combined tangential and normal injection slot scheme with finite lip thickness and they concluded the following; 1) the effectiveness increases with increasing the velocity ratio, lip length, and open area ratio, 2) for a given coolant flow rate, the influence of tangential to normal momentum ratio increase is small and tends to improve the effectiveness, and 3) a single row of tangential holes with small pitch to diameter ratio results in better performance than combined tangential and normal holes.

Shaped-discrete-hole schemes were proposed to sustain reasonable material strength and good film cooling performance at the same time. Numerous designs were proposed and investigated in literature. An Attempt to approach slot injection performance, Sargison et al. [5], [6] proposed and experimentally investigated the film cooling performance of a converging-slot-hole (console), Fig. 1a, scheme over a flat plate and a gas turbine transonic vane. The scheme entry section is circular and then expands in the lateral direction and converges in the streamwise direction. For optimal lateral coverage they designed the scheme with no gabs between the holes exits. The console scheme showed good effectiveness performance on both flat plate and vane surface. To improve the coolant lateral spreading of the console scheme, Liu et al. [7] proposed the waist-shaped console scheme. The

waist pushes the coolant towards the sides of the scheme in order to help sustain a better coverage to the area between the holes. Fan-shaped and laidback fan-shaped schemes were proposed and investigated numerous times in literature at a variety of flow and geometrical conditions on both flat plate and actual airfoil geometries by Thole et al. [8], Gritsch et al.[9], [10], and many others.

Besides proposing new designs of shaped scheme many investigations were carried out to enhance the performance of the existing designs. One of the schemes that were subjected to many investigations is the circular scheme. The importance of this scheme comes from its simplicity in manufacturing and its minor effect on the component material strength, compared to shaped schemes. The disadvantages of the circular scheme could be summarized in its low film cooling effectiveness and its bad lateral jet spreading. Among the factors that affect the performance of the circular scheme is the presence of a strong Counter Rotating Vortex Pair (CRVP) on both sides of the jet. The strength of the CRVP vortex is proportional to the velocity gradient between the jet and the main stream which is a maximum in the case of circular schemes, compared to the shaped cases. To decrease the CRVP intensity, the generation of another vortex opposite in direction to that of the CRVP was proofed to be a good solution. Heidmann and Ekkad [11] presented numerical investigations of an anti-vortex scheme, Fig. 1b. In their design, two side holes were drilled, on both sides of the main circular hole and intersect with it. The interaction between the flows of the side holes of adjacent main holes generates the targeted vortex. They examined different locations of the side holes in relation with the main hole. Enhanced film cooling effectiveness was obtained by the new design compared to the base line case, the circular scheme. A similar design was proposed by Li and Zhang [12]. The scheme they proposed is a circular scheme with one inlet and double outlet, Fig. 1c. Noticeable enhancement in the film cooling effectiveness was observed. Kusterer et al. [13] proposed the double-jet ejection film cooling. They proposed the placement of two compound circular holes in relation with each other so that the vortex resulting from the first hole is in opposite direction to that resulting from the second hole, Fig. 1d. They investigated different configuration and they obtained great enhancement in the film cooling effectiveness. Li et al. [14] proposed a different approach to control the CRVP intensity. They proposed the use of internal inserts with the circular scheme to control the velocity distribution at the exit and hence the CRVP intensity. They presented excellent enhancement in the film cooling effectiveness at different blowing ratios. They also proofed that caution must be considered while shaping the scheme exit to ensure that the CRVP intensity is at minimum.

Combining the jet impingement benefits and film cooling in one scheme, the Louver scheme was first proposed by Immarigeon and Hassan [15]. The Louver scheme is a shaped scheme with an internal 90° bend, circular hole followed by a horizontal slot. The main purpose of the internal bend inside the louver scheme is to protect the region upstream the injection location. Zhang and Hassan

[16], [17] numerically investigated the film effectiveness of one row and two rows of a modified louver scheme over a flat plate. Ghorab et al. [18], Elnady et al. [19] experimentally examined the performance of the louver scheme over a flat plate, and an actual gas turbine vane, respectively. In all previous investigations, the louver scheme showed enhanced film cooling performance, compared to other film cooling schemes.

All previously conducted researches to investigate the film cooling performance downstream the louver scheme were based on the design shown in Fig. 4a. The shape of the hole exit in connection with the design of the internal slot are expected to have significant contribution on the film cooling effectiveness. Changing the scheme exit area and the interface line between the scheme exit and the test surface changes the interaction nature between the supplied jet and the main stream and hence affects the film cooling performance of the scheme. Meanwhile, it was expected that the internal bend has a contribution on the film cooling performance of the louver scheme by affecting the jet momentum direction at the scheme exit. In order to investigate the effect of such two points, three separate schemes were manufactured. The first, is the old louver Fig. 2a, has an oblong cross section slot and a 30° inclined shaped exit with 10° lateral expansion angle and 5° forward stream wise inclination angle and 5° backward streamwise inclination angle. The interface between the exit and the test area is a straight line. It will be named all over this study as Louver with Straight Exit (LSE). The second design, the modified louver Fig. 2b, has a circular cross section slot, to facilitate the manufacturing of the scheme, and a 25° inclined shaped exit with 10° lateral expansion angles and without streamwise diffusion angles. The interface between the exit and the test area is a circular arc. It will be named all over this study as Louver with Curved Exit (LCE). The third, Fig. 2c, is a shaped scheme with the same exit geometry as the LCE but without the internal bend. The latter will be referred to as Shaped WithOut Bend (SWOB). The film cooling performance of the proposed designs will be investigated at three different blowing ratios, 0.5, 1.0 and 1.5, a density ratio of 0.93, a Reynolds Number of $1.24E+5$, based on the free stream velocity and the main duct hydraulic diameter, and a turbulence intensity of 8.5. The blowing ratio is calculated based on the base diameter of the LSE scheme (i.e. the amount of coolant supplied is the same as that supplied to a circular hole with the same base diameter of LSE scheme).

2. EXPERIMENTAL FACILITY AND METHODOLOGY

2.1. Test Facility and Test Section

Figure 3 is a schematic diagram of the subsonic wind tunnel and its subcomponent established at Concordia University. The wind tunnel is composed of three main systems; mechanical, electronic, and thermography systems.

2.1.1. The Mechanical System

The mechanical system includes the supply loops of the main and secondary air streams, the flow meters, the heaters, and the pressure gauges and regulators. The main and secondary air streams are provided by a compressed air tank whose pressure is regulated to 7 bars and its volume is 3.7 m³. The main stream needs larger tanks to be heated but such tanks cannot be installed because of space limitations. Throughout this study, the secondary stream is heated instead. Each flow loop is provided with flow control valves, pressure regulators and flow meters. To eliminate any fluctuations in the main stream, a divergent-convergent nozzle is installed in the main flow path. A fine grid mesh is installed at the exit of the divergent-convergent nozzle so that a turbulence intensity of 8.5% is maintained. For the secondary stream to be heated an air heater with a maximum capacity of 1.2kW is used. A 3-way solenoid valve is used to by-pass the flow during the heating process before it is converted to the test section.

2.1.2. The Thermography System

The thermography system includes the CCD camera, the Light source, the light supply and the frame gripper. A 3CCD digital (IK-TF7C) Toshiba camera is used to capture the colored images of the TLC downstream the injection holes at a rate of 5 fps. An NI PCIE-1340 dual frame gripper is used to transfer the captured images from the camera to the work station. A variable intensity light source provided with optical fiber cables is used to supply the required light intensity to the test surface. The captured, Red-Green-Blue (RGB) images are saved in Tagged Image File Format (TIFF) with a size of 1024 × 768 pixels. The images are then fed into an in-house MATLAB module to map them to the corresponding temperature distributions through an in-situ calibration process.

2.1.3. The Electronic System

The electronic system includes the work station and the data acquisition (DAQ) system. A Pentium 4 Dell Precision workstation with 3.75 GHz CPU, 3.25 GB of RAMs and 250 GB hard drive is used. An M-series NI DAQ system is used to capture the signal from all instruments and sensors (pressure, flow and temperature). An in-house built Labview code is used to manage the test facility by controlling the timing of valves opening and closing and recording of temperatures, pressures, flow rates and the captured images.

2.1.4. Test Section

The test section used in this study is a flat plate test section, Fig. 4. The main test section is manufactured from a transparent material to facilitate imaging through the walls. The cross section of the test section is 99.0mm × 54.0mm and its length is 550.0mm. The bottom plate was manufactured

in two pieces, the first is the main body of the plate and the second is the region containing the film cooling schemes under investigation. This allows replacing the cooling scheme without disassembling the whole bottom plate, thereby minimizing the time of setup and the cost of manufacturing. The film cooling schemes were located at a distance of 200.0mm from the test section inlet to allow the main stream to develop before it interacts with the secondary stream. A plenum with internal dimensions of 65.0mm × 66.8mm × 45.0mm was used to supply the secondary stream to the test section.

More details about the test facility and the imaging technique are available in Hassan [20].

2.2. TLC Calibration

Narrow band TLC sheets (R25C5W) with a temperature range 5°C, from 20°C to 25°C, are used to map the temperature distribution along the target area. The hue angle method was used to quantify the observed color to the material temperature. Details of this method were described by Ghorab et al [18]. For the TLC to be calibrated, a special calibration target was manufactured of Aluminum, to ensure homogeneous surface temperature distribution. Two heaters (Omega, KH-308/2P), with a maximum power output of 1.55 W/cm², were used to apply uniform heat flux to the TLC sheet during the calibration process. T-type thermocouples were installed in various places over the surface to capture the average surface temperature. By slightly increasing the power supplied to the heater and waiting proper time to achieve steady state, N-number of images and the corresponding surface temperatures are captured. The surface area of the TLC sheet is divided into Regions of Interest (ROI) and each ROI is a square of n×n pixels. During the analysis each ROI is considered separately. Using an in-house built MATLAB codes, any further captured images during the experiments are converted to temperature distributions. The calibration of the TLC is carried out every time the set-up is changed and intermediately between tests, every few days, to ensure that the camera and light positions did not changed. More details about the calibration procedure could be found in Hassan [20].

2.3. Data Reduction

The solution of the one dimension heat conduction Eq. (2.1), using the initial and boundary conditions in Eq. (2.2), semi-infinite solid assumption, gives the system temperature as a function of the heat transfer coefficient and the thermal properties of the vane material, Eq. (2.3),

$$\rho C_p \frac{\partial T}{\partial t} = \frac{\partial}{\partial x} \left(k \frac{\partial T}{\partial x} \right) \quad (2.2)$$

$$\left. \begin{aligned} @ t = 0, \quad T &= T_i \\ @ x = 0 \quad h(T_w - T_f) &= -k \frac{\partial T}{\partial x} \end{aligned} \right\} \quad (2.2)$$

$$@ x = \infty \quad T = T_i \quad (2.1)$$

$$\frac{T_w - T_i}{T_f - T_i} = 1 - \exp\left(\frac{h^2 \alpha t}{k^2}\right) \operatorname{erfc}\left(\frac{h\sqrt{\alpha t}}{k}\right) \quad (2.3)$$

Where, the wall temperature, T_w , the initial temperature, T_i , and the mainstream temperature, T_m , are measured using thermocouples and the TLC sheet. The film temperature, T_f , could be calculated as a function of the coolant temperature, T_c , the mainstream temperature, and the film cooling effectiveness, η , Eq. (2.4);

$$T_f = \eta T_c + T_m (1 - \eta)$$

Equations (2.3) & (2.4) are then reduced to one equation in two variables, h and η , Eq. (2.4)

$$T_w - T_i = \left[1 - \exp\left(\frac{h^2 \alpha t}{k^2}\right) \operatorname{erfc}\left(\frac{h\sqrt{\alpha t}}{k}\right)\right] * [\eta(T_c - T_m) + T_m - T_i]$$

A single transient test of 60 seconds at a rate of 5 Hz for a total of 300 images (N) is considered in this study to solve Eq. (2.5) for every ROI using the non-linear least squares regression method for the two unknown variables, h and η . More details about the solution technique are available in Hassan [20].

Uncertainty analysis is based on 95% confident level and determined using the methodology of Klein and McClintock [21]. The average estimated uncertainties in the measured temperatures (thermocouples and TLC), flow rate, pressure, thermal diffusivity and thermal conductivity, are; $\pm 0.5^\circ\text{C}$ ($\pm 2\%$), $\pm 3\%$, $\pm 3\%$, $\pm 2\%$ and $\pm 3\%$, respectively. The corresponding uncertainties in blowing ratio, effectiveness, HTC and NHFR are; $\pm 6\%$, $\pm 8\%$, $\pm 12\%$ and $\pm 14\%$, respectively. Details of the uncertainty analysis are available in the work of Hassan [20].

2.4. Validation of Test Facility and Methodology

The work of Wright et al. [22] was chosen to validate the present work. The reasons behind choosing the work of Wright et al. [22] are; 1) they applied test conditions that are very close to those applied throughout the present study, 2) they presented acceptable validation of their work with previous works, 3) they implemented a different thermography technique, the transient Pressure Sensitive Paint (PSP) technique, from the one implemented throughout the present study, the transient TLC technique. The third reason allows verifying the effect of changing the thermography technique on the results. Throughout their analysis, Wright et al. (2011) applied a relatively low Reynolds number, $0.7E5$. Such range of Reynolds numbers is accompanied with high uncertainty level in the measured parameters using the current test facility. This is due to two reasons; the first is related to the TLC sheets used for wall temperature measurements and the second is related to a design problem in the test target. The presence of the TLC sheet edge in front of the scheme exit results in an enhanced jet distribution in the lateral direction which accordingly reduces the centerline effectiveness. To overcome this challenge, the TLC sheet was impeded in a groove machined on the

surface in order to integrate with the surface and reduce the disturbance. However, some complications incurred from the presence of the groove and as a result, the surface was flushed and the groove was removed again. Moreover, the test section is designed so that the film cooling scheme can be replaced without changing the whole test target in order to minimize efforts during experiments and manufacturing costs. This resulted in the presence of a small gap between the location of the scheme exit and the TLC sheet which works as an obstacle in front of the injection schemes. The impact of the previously mentioned obstacle decays with increasing Reynolds number due to the enhanced jets strength.

Figure 5 is a comparison of the centerline and spanwise-averaged effectiveness of one row of circular hole schemes over a flat plate with the work of Wright et al. [22]. From the figure, good agreement is noticeable at both blowing ratios, for centerline and laterally averaged effectiveness, along the downstream area. The agreement in the average effectiveness close to the injection location at $Br = 1.0$ is not as good as the one obtained at $Br = 0.5$. This is due to the presence of jet lift off at $Br = 1.0$ and the presence of the previously mentioned obstacles in front of the injection location. The impact of the TLC edge is represented in the enhanced effectiveness close to the injection location, $x/d < 3.0$, as the TLC sheet thickness enhances the attachment of the jet to the surface, because it reduces the actual vertical penetration distance of the jet, perpendicular to the surface.

3. RESULTS AND DISCUSSIONS

3.1. Film Cooling Effectiveness

Figure 6 is a sample of the test surface images captured during the experiments downstream different schemes at different blowing ratios. The image in the figure is the last captured image during different tests, image # 300. The purpose of this figure is to show the secondary jet traces as captured by the TLC sheets before converting it to temperature distribution and hence to the corresponding effectiveness and HTC. In front of each image, the location, shape and relative size of the injection scheme exit is shown as well. At $Br = 0.5$, Fig. 6a, the jet traces downstream the three cases are very close to each other. This is attributed to the low coolant amount supplied from the three schemes. As a result, changing the scheme exit does not have significant effect on the interaction between the main and the secondary streams even with the presence of different schemes exit. At $Br = 1.0$ and 1.5 , the case is different. The jet traces downstream the LCE and the SWOB cases are covering larger areas in the downstream direction, compared to the LSE case. The scheme exit area in the case of LSE is large, compared to the two other cases. The increase in the coolant amount accompanying the blowing ratio increase does not result in significant changes in the jet strength downstream the LSE

case because it is being calculated based on the scheme base diameter which is very small compared to the scheme exit area. However, the secondary jets downstream the LCE and the SWOB cases become stronger by blowing ratio increase and hence penetrate deeper inside the mainstream. The 5° reduction in the scheme exit inclination angles in the cases of LCE and SWOB compared to the LSE case helps reduce the perpendicular penetration of the secondary jets as well. Meanwhile, the effect of changing the scheme exit shape results in difference in the interaction nature between the main and the secondary streams. This in turn helps enhance the surface coverage downstream the LCE and the SWOB cases. The latter is clear from the dark colors away from the images centerline downstream LCE and SWOB schemes, compared to the light image colors downstream the LSE scheme.

Figures 7, 8 and 9 are the quantitative effectiveness comparisons between the three schemes at different blowing ratios. The effectiveness comparisons at $Br = 0.5$ are shown in Fig. 7. From the effectiveness contours, Fig. 7a, the information observed from Fig. 6 is confirmed. The secondary jets downstream the three cases almost have the same properties. Very slight enhancement in the effectiveness is observable in the cases of LCE and SWOB compared to the case of LSE. Meanwhile, the Effectiveness downstream the SWOB case is a little bit enhanced compared to the LCE case. In general, the differences between the three cases are minimal and concentrated around the centerline as shown from the centerline effectiveness comparison in Fig. 7b. In the figure, the centerline effectiveness downstream the SWOB is higher than the centerline effectiveness downstream the LCE scheme from the beginning of the region of interest till $x/d = 10$. The centerline effectiveness remains the same downstream the three schemes for the rest of the region of interest. The enhancement in the centerline effectiveness observed in Fig. 7b is not apparent in Fig. 7c, the spanwise-averaged effectiveness comparison. As mentioned earlier, the secondary jets downstream the three schemes are very weak at the low blowing ratio case, $Br = 0.5$. As a result the interaction between the main and the secondary streams and the effect of the scheme exit design are at minimum in all cases. The larger scheme exit in the case of the LSE scheme helps distribute the coolant better in the lateral direction. This resulted in the minor reduction in the centerline effectiveness; however, it offered the same spanwise-averaged effectiveness as observed downstream the two other cases. Contrarily, the curved exit of the LCE and the SWOB schemes concentrated part of the secondary jet in front of the scheme exit with minor reduction in the lateral jet spreading.

The differences in the effectiveness performance between different cases are clear in Fig. 8. The effectiveness contours, Fig. 8a, shows the big enhancement in the secondary jet traces downstream the SWOB and LCE cases, compared to the LSE case. When the effectiveness contours of the LSE and the LCE are compared, the enhancement downstream the LCE scheme is observable in both spanwise and streamwise directions. The enhanced performance of the LCE is due to many factors; 1)

the reduced LCE scheme exit inclination angle, 25° instead of an averaged 30° in the case of the LSE scheme. Smaller inclination angle results in a larger x-momentum component and smaller y-momentum component. The latter results in better secondary jet attachment to the surface, and hence reduction in the mixing between the two streams. 2) The curved LCE scheme exit results in smoothed jet supply. This reduces the interaction between the jet and the main stream and as a result reduces the intensity of the Counter Rotating Vortex Pair (CRVP). The presence of the CRVP results in enhanced mixing between the two streams and allows the mainstream to penetrate beneath the secondary stream at high blowing ratios. 3) The area of the LCE exit is smaller than that of that of the LSE one. A smaller scheme exit area results in a stronger jet that is capable of withstanding the effects of the vortices generated from the interaction between the two streams better than the larger exit area one. However, increasing the scheme exit area helps reduce the jet perpendicular momentum.

The similarity in the effectiveness contours downstream the LCE and the SWOB schemes that is clear in Fig. 8a is an indication that the internal louver bend does not have a contribution on the resulting effectiveness downstream the scheme. Previous louver investigations showed enhanced effectiveness performance downstream the louver scheme, when compared to other schemes. Researchers related part of the enhancement to the presence of the internal bend. In the present study, the LCE and SWOB schemes were designed identical, except the presence of the internal bend in the case of the LCE scheme. The centerline and spanwise-average effectiveness performance, Figs. 8b and c, supports the information observed from the effectiveness contours. The centerline and spanwise-averaged effectiveness downstream the two schemes are almost identical all over the region of interest. Meanwhile, very slight enhancement in the centerline effectiveness is observable far downstream the injection location in the case of SWOB scheme compared to the case of LCE scheme.

Similar effectiveness performance to that observed with $Br = 1.0$ is observable from Fig. 9 for $Br = 1.5$. The enhancement in the effectiveness downstream the LCE and the SWOB cases is clear when compared to the LSE case. If the effectiveness contours downstream the LSE scheme in Figs. 7a, 8a and 9a are compared; enhancement in the effectiveness is noticeable around the scheme centerline with blowing ratio increase and is accompanied with minor reduction in the effectiveness in the spanwise direction. This is attributed to the enhanced vortices on the sides of the secondary jet with blowing ratio increase while its strength is being increased around the centerline due to the increased coolant amount. The enhanced jet strength allows it to penetrate deeper inside the mainstream. Downstream the LCE and SWOB schemes the curved scheme exit in conjunction with the small inclination angle led to enhanced effectiveness in both streamwise and spanwise directions with blowing ratio increase. Besides, slight enhancement in the effectiveness is observable downstream the SWOB case in comparison to the LCE case especially around the centerline. The jet supplied from

the LCE scheme is subjected to impingement effects inside the scheme which results in small reduction in the jet temperature, compared to the SWOB case. The reduction in the jet temperature is minimum in the present study because the material from which the scheme is manufactured has very low thermal conductivity. In real cases, the impingement effects are expected to be more severe. The centerline and spanwise-averaged effectiveness, Figs. 9a and b, supports the information observed from the contours.

Figure 10, presents the effect of blowing ratio variation on the spanwise-averaged effectiveness of different schemes. The change in the spanwise-averaged effectiveness downstream the LSE case is very small as is clear from Fig. 10a. As mentioned earlier, this is attributed to the method used for blowing ratio calculation implemented during the present study. The blowing ratio is calculated based on the louver scheme base diameter. As a result, the change in the coolant amount accompanying the blowing ratio increase is small, in regard to the large scheme exit area. Removing the diffusion angles and adding the curvature to the scheme exit design as in the cases of the LCE and SWOB are the reasons behind the reduction occurred in the schemes exit areas. The latter magnified the effect of increasing the coolant amount with blowing ratio increase, as observed from Figs. 10b and c. A clear observation in these two figures is that the effectiveness enhancement due to blowing ration increase from 0.5 to 1.0 is higher than the effectiveness enhancement due to blowing ratio increase from 1.0 to 1.5. In general, increasing the coolant amount by increasing the blowing ratio is accompanied with enhanced vortices strength. The enhancement in the vortices strength is exponentially proportional to the blowing ratio increase as was proved by Hassan and Hassan [23]. This is enough to overcome a significant portion of the effectiveness enhancement due to the increased coolant amount.

3.2. Film Cooling Heat Transfer Coefficient

To clarify the effect varying the injection scheme design on the HTC performance, the HTC performance is presented as a ratio of the HTC with film cooling to that without film cooling (h_o). The calibration target was used to determine the HTC distribution over the surface without film cooling. A uniform heat flux, q'' , was applied using the heater. The corresponding steady state wall temperature distribution, T_w , was recorded using the TLC sheet that was placed on top of the heater. Thermocouples were used to record the main stream temperature, T_m . Using Newton's law of convection, Eq. (3.1), h_o is calculated as follows:

$$h_o = q'' / (T_w - T_m) \quad (3.1)$$

The HTC ratio contours downstream the three schemes are presented in Fig. 11. From the contours it is clear that changing the scheme exit design does not have a significant effect on the

resulting HTC ratio. The main clear difference in the HTC ratio is apparent when the contours of the same scheme are compared at different blowing ratios, as the HTC ratio increases slightly with blowing ratio increase. The blue spot in the middle of the contours is a result of a small dark zone in the HTC without film cooling. Meanwhile, the dark red zones on the sides of the contours close to the end of the region of interest do not present the actual HTC ratio in these zones. Such regions are so far from the injection scheme and as a result the temperature build up is not homogeneous and this leads to the shown bias in the HTC. Increasing the blowing ratio leads to strengthened secondary jets and this helps minimize the bias zones. This is clear from the figure as the red zones shrinks with blowing ratio increase.

4. CONCLUSIONS AND RECOMMENDATIONS

The effect of louver scheme exit design and the presence of internal 90° bend on the resulting net film cooling performance were investigated using the transient TLC technique. The Louver scheme is a shaped scheme with an internal 90° bend, circular hole followed by a horizontal slot, which adds the impingement cooling benefits to the enhanced film cooling performance of shaped schemes. In order to conduct the present investigations, three different schemes were manufactured. The first is a Louver with Straight Exit (LSE) and has an oblong cross section slot, a 30° inclined shaped exit with 10° lateral expansion angle and 5° forward and backward diffusion angles. The interface between the exit and the test area is a straight line. The second is a Louver with Curved Exit (LCE) and has a circular cross section slot, to facilitate the manufacturing of the scheme, a 25° inclined shaped exit with 10° lateral expansion angles and without streamwise diffusion angles. The interface between the exit and the test area is a circular arc. The third is a shaped scheme with the same exit geometry as the LCE but without the internal bend (SWOB). The film cooling performance of the proposed designs was investigated at three different blowing ratios, 0.5, 1.0 and 1.5, a density ratio of 0.93, a Reynolds Number of $1.24E+5$, based on the free stream velocity and the main duct hydraulic diameter, and a turbulence intensity of 8.5. The blowing ratio is calculated based on the base diameter of the LSE scheme. (i.e. the amount of coolant supplied is the same as that supplied to a circular hole with the same base diameter of LSE scheme)

The investigations showed that the scheme exit design has a significant effect on the resulting effectiveness as it affects the interaction nature between the main and the secondary streams. This was clear during the investigations through the enhanced effectiveness performance downstream the louver scheme with curved exit design, compared to the louver with straight exit. Also, adding a 90° internal bend to the shaped scheme design for impingement cooling purposes does not have a contribution on the scheme film cooling performance. Changing the film cooling scheme design did

not affect the resulting heat transfer coefficient distribution significantly. This was attributed to the small change in the supplied coolant mass due to using the scheme base diameter for blowing ratio calculations.

ACKNOWLEDGEMENTS

The author acknowledges Concordia University for allowing the use of the gas turbines experimental test facility inside their labs.

NOMENCLATURE

Symbols

Br	blowing ratio ($\rho_j u_j / \rho_m u_m$)
d	diameter of film hole (m)
d_h	hydraulic diameter of the main duct
DR	density ratio (ρ_j / ρ_m)
h	heat transfer coefficient ($\text{W}/\text{m}^2 \cdot \text{K}$)
K	thermal conductivity of plate ($\text{W}/\text{m} \cdot \text{K}$)
p	film hole pitch (m)
q	heat transfer flux (W/m^2)
Re	Reynolds number ($\rho D_h U_m / \mu$)
T	temperature (K)
t	time (s)
\bar{T}_w	average wall temperature (K)
U_m	normal main stream velocity in x direction (m/s)
α	Thermal diffusivity (m^2/s), = ($k/\rho C_p$)
η	local film cooling effectiveness ($(T_f - T_m) / (T_j - T_m)$).
η_{avg}	Spanwise-averaged film cooling effectiveness.
ho	heat transfer coefficient without film cooling ($\text{W}/\text{m}^2 \cdot \text{K}$)
ρ	density (kg/m^3)

Subscripts and superscripts

avg	average
c	centerline
f	Film
i	initial
j	Jet

m main stream

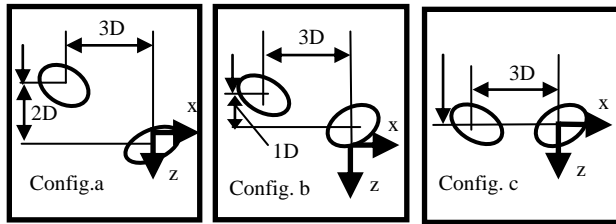
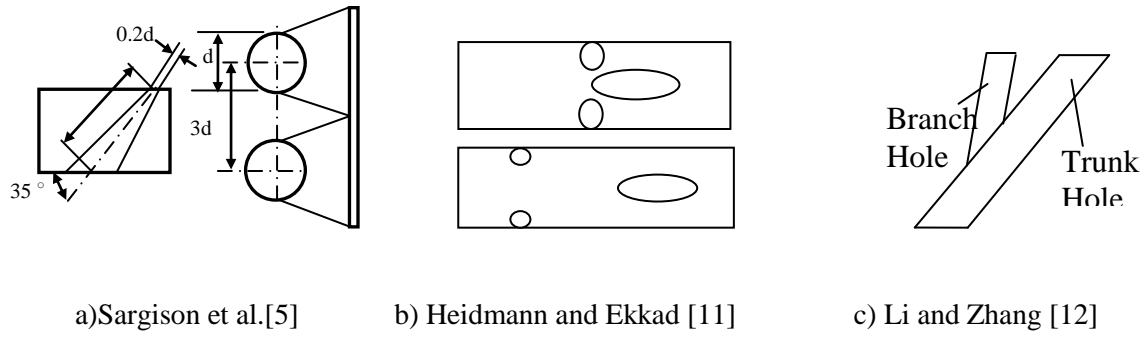
Abbreviations

CRVP	Counter Rotating Vortex Pair
HTC	Heat Transfer Coefficient
LCE	Louver with Curved Exit
LSE	Louver with Straight Exit
SWOB	Shaped WithOut Bend
TLC	Thermochromic Liquid Crystal

REFERENCES

- [1] R.J. Goldstein, R.B. Rask and E.R.G. Eckert, "Film Cooling With Helium Injection into an Incompressible Air Flow", *Int. J. Heat Mass Transfer*, 9 (1966) 1341-1350.
- [2] J.P. Hartnett, R.C. Birkebak and E.R.G. Eckert, "Velocity distributions, temperature distributions, effectiveness and heat transfer for air injected through a tangential slot into a turbulent boundary layer", *J. Heat Transfer*, 83 (1961) 293–306.
- [3] K. Wiegardt, "Hot-Air Discharge for De-icing", AAF Translation, Report No. F-TS-glg-Re, (1946), Wright Field.
- [4] C.O. Folayan and J.H. Whitelaw, "Effectiveness of combined tangential and normal film cooling with finite", *Proceedings of the ASME*, (1976) 76-HT-30.
- [5] J.E. Sargison, S.M. Guo, M.L.G. Oldfield, G.D. Lock and A.J. Rawlinson, "A converging slot-hole film-cooling geometry-Part I: Low-speed flat-plate heat transfer and loss", *ASME J. of Turbomachinery*, 124/3 (2002) 453-460.
- [6] J.E. Sargison, S.M. Guo, M.L.G. Oldfield, G.D. Lock, and A. J. Rawlinson, "A converging slot-hole film-cooling geometry-Part II: Transonic nozzle guide vane heat transfer and loss", *ASME J. of Turbomachinery*, 124/3 (2002) 461-471.
- [7] C.L. Liu, H.R. Zhu, J.T. Bai, and D.C. Xu, "Experimental and numerical investigation on the film cooling of waist-shaped slot holes comparing with converging slot holes", *ASME J. of Turbomachinery*, 134/1 (2012) 011021-11.
- [8] K. Thole, M. Gritsch, A. Schulz and S. Wittig, "Flow field measurements for film-cooling holes with expanded exits", *Proceedings of the ASME* (1996).
- [9] M. Gritsch, W. Colban, H. Schar and K. Dobbeling, "Effect of hole geometry on the thermal performance of fan-shaped film cooling holes", *ASME J. of Turbomachinery*, 127(2005) 718-25.

- [10] M. Gritsch, A. Schulz and S. Wittig, "Adiabatic wall effectiveness measurements of film-cooling holes with expanded exits", ASME J. of Turbomachinery, 120 (1998) 549-556.
- [11] J. D. Heidmann, and S. Ekkad, "A novel antivortex turbine film-cooling hole concept". Journal of Turbomachinery, 2008, vol. 130 (3): pp. 031020-1.
- [12] G.-C. Li and W. Zhang, "Improving film cooling performance by using one-inlet and double-outlet hole". Journal of Thermal Science. vol. 19 (5): p. 430-437.
- [13] K. Kusterer, D. Bohn, T. Sugimoto and R. Tanaka "Double-jet ejection of cooling air for improved film cooling", Journal of Turbomachinery, 2007, vol. 129 (4): p. 809-815.
- [14] H. M. Li, O. Hassan and I. Hassan, "the effects of counter rotating vortex pair's intensity on film cooling effectiveness", ASME, IMECE2011-64400
- [15] A. Immarigeon and I. Hassan, "An advanced impingement/film cooling scheme for gas turbines – numerical study". International Journal of Numerical Methods for Heat & Fluid Flow, 2006, vol. 16 (4), pp. 470-493.
- [16] X.Z. Zhang and I. Hassan, "Film cooling effectiveness of an advanced-louver cooling scheme for gas turbines", J. of Thermophysics and Heat Transfer, 20 (2006) 754-763.
- [17] X.Z. Zhang and I. Hassan, "Numerical investigation of heat transfer on film cooling with shaped holes", Int. J. of Numerical Methods for Heat and Fluid Flow, 16 (2006) 848-69.
- [18] M.G. Ghorab, I.G. Hassan, and T.Lucas, "An experimental investigation of film cooling performance of louver scheme", Int. J. of Heat and Mass Transfer, 54 (2011) 1387-1399.
- [19] T. Elnady, W. Saleh, I. Hassan, L. Kadem and T. Lucas, "Experimental investigations of louver cooling scheme on gas turbine vane pressure side", Proceedings of International Heat Transfer Conference, (2010) IHTC14-22398.
- [20] O. Hassan, "Thermal and Flow Field Investigations of the Film Cooling Performance of A Micro-Tangential-Jet Scheme on Gas Turbine Components", PhD Thesis, Concordia University, Canada (2013).
- [21] S. J. Kline and F.A. McClintock, "Describing uncertainties in single sample experiments" ASME Mechanical Engineering, 1975, pp. 3-8.
- [22] L.M. Wright, S.T. McClain and M.D. Clemenson, "Effect of density ratio on flat plate film cooling with shaped holes using PSP", ASME J. of Turbomachinery, 133(2011) 041011-1.
- [23] O. Hassan, and I. Hassan, "Experimental Flow Field Investigations Downstream a Scaled-Up Micro-Tangential-Jet Scheme Using the PIV Technique", ASME Journal of Fluids Engineering (2014) 136 (7), 071204.



d) Kusterer et al. [13]

Figure 1, Sample of previously proposed shaped schemes

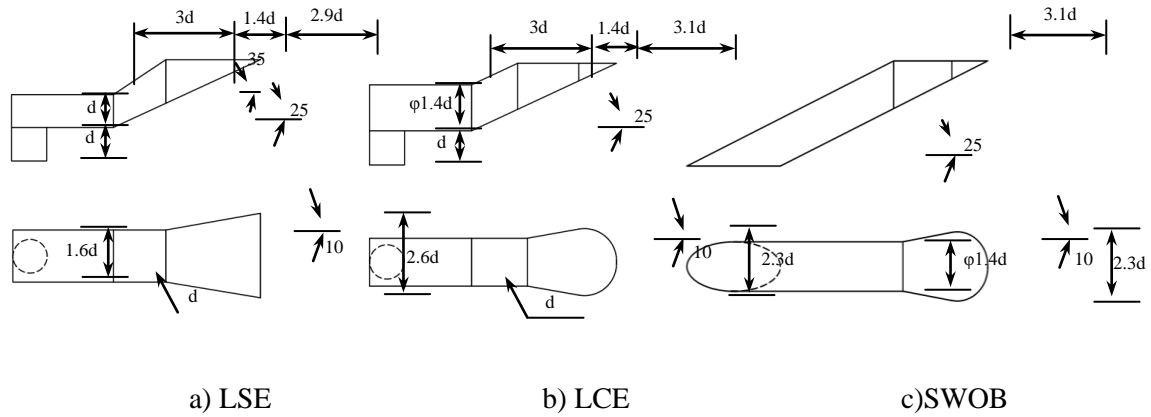


Figure 2, Schemes geometrical properties

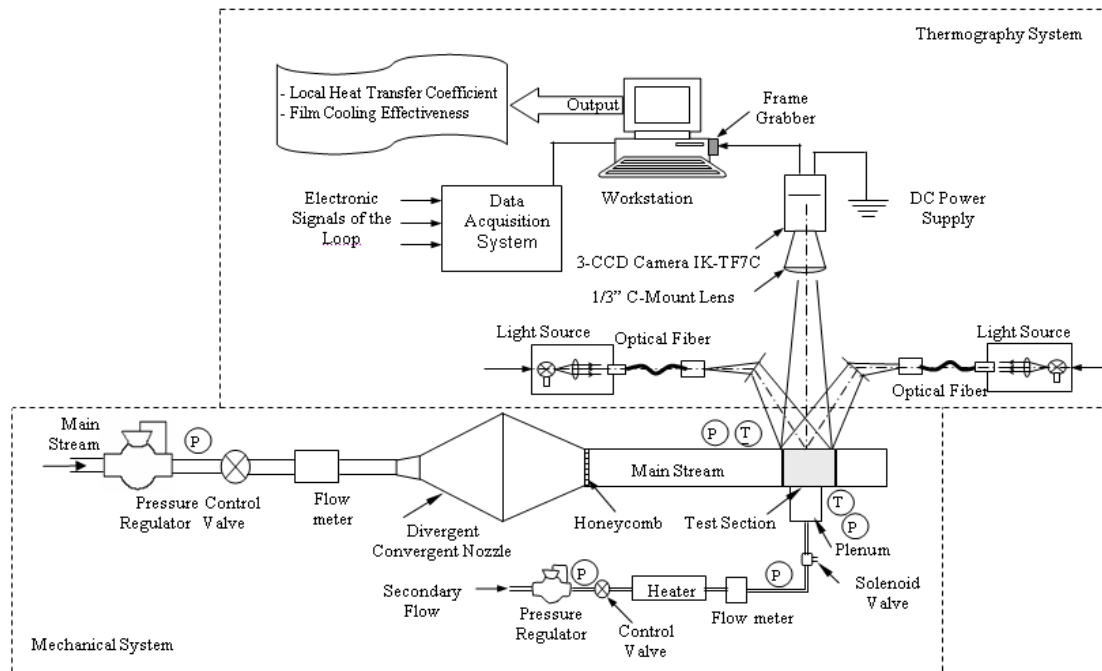


Figure 3, Schematic diagram of the film cooling test rig

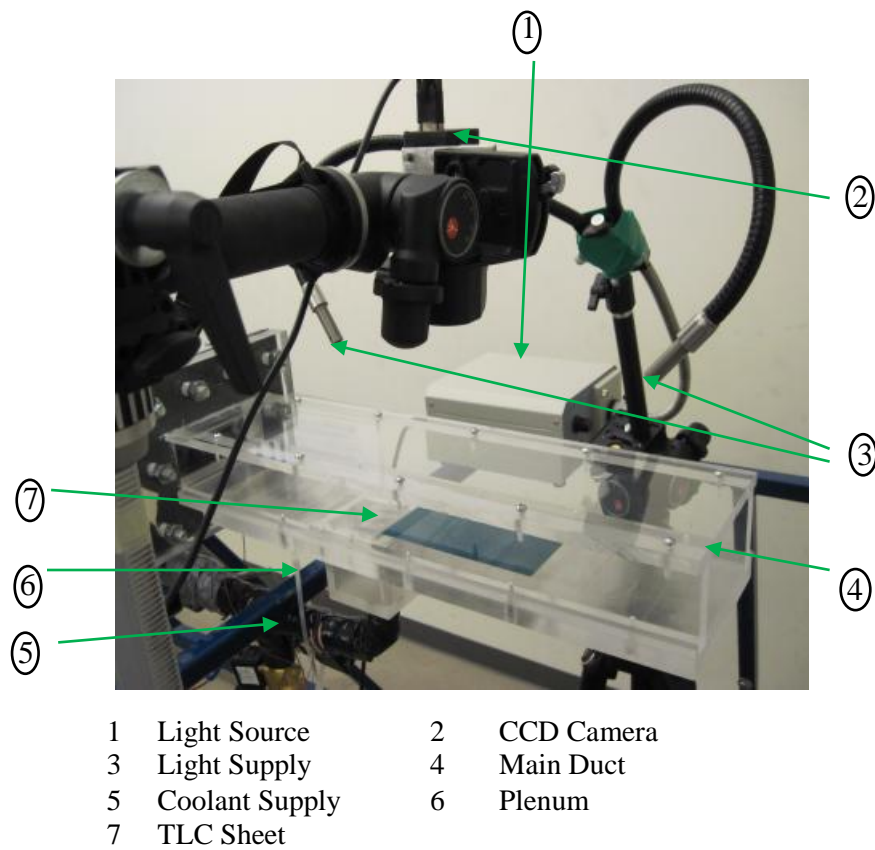


Figure 4, Flat plate test section details

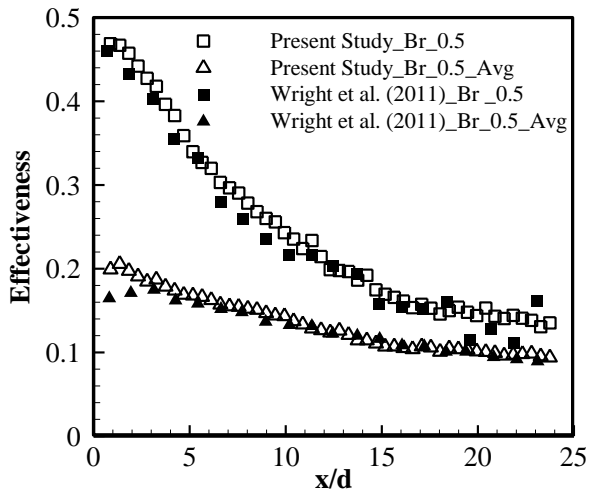
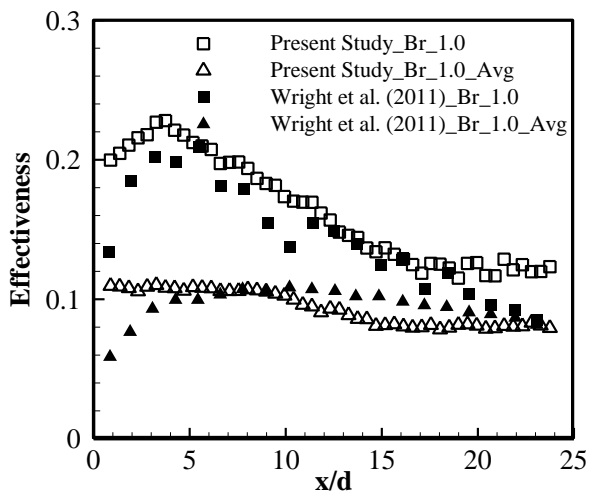
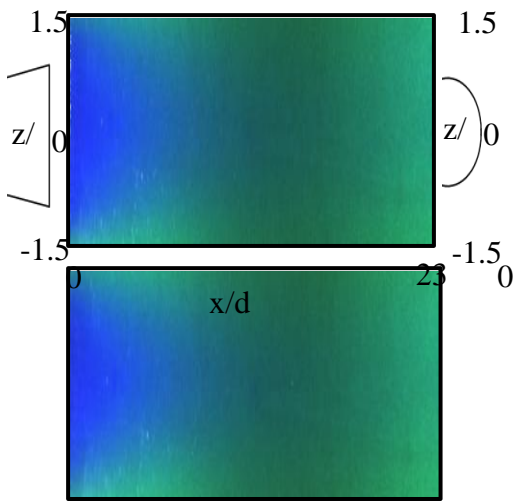
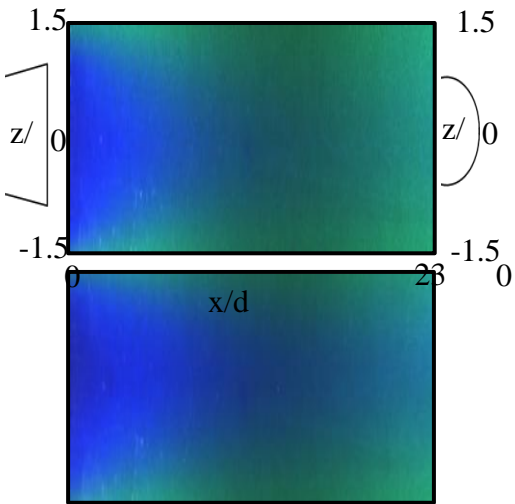
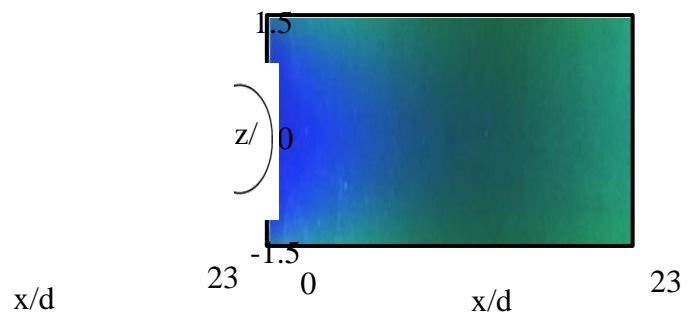
a) $Br = 0.5$ b) $Br = 1.0$

Figure 5, Centerline and Spanwise-averaged effectiveness comparison downstream one row of circular hole schemes between present study and the work of Wright et al. [22]



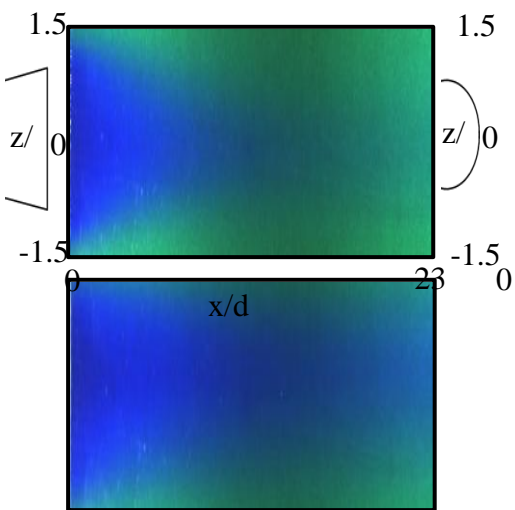
a) $Br = 0.5$



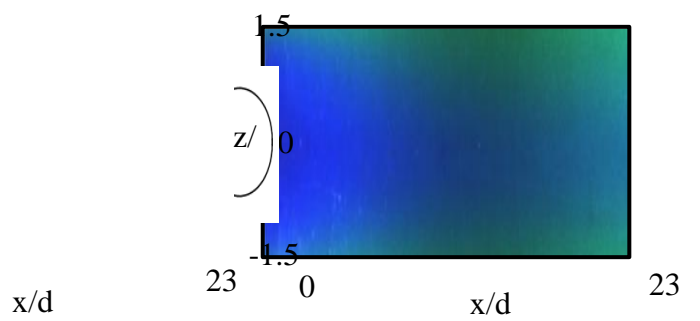
b) $Br =$

=

1.0



c) $Br = 1.5$

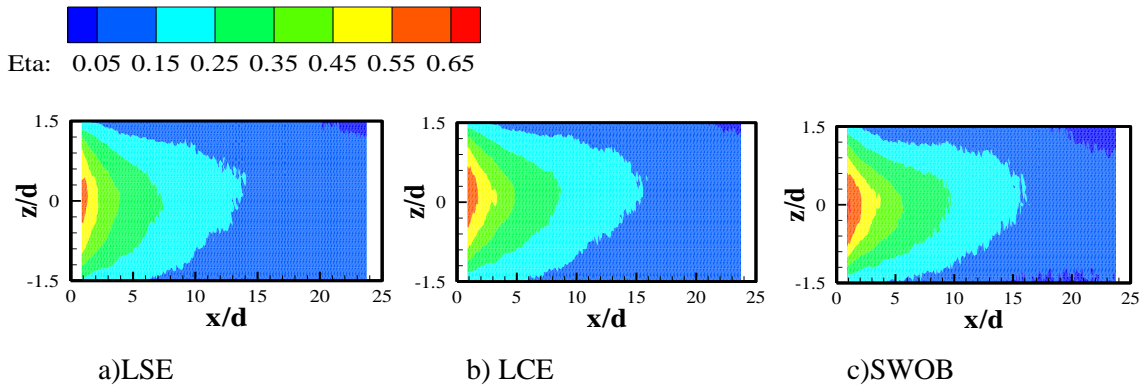


LSE

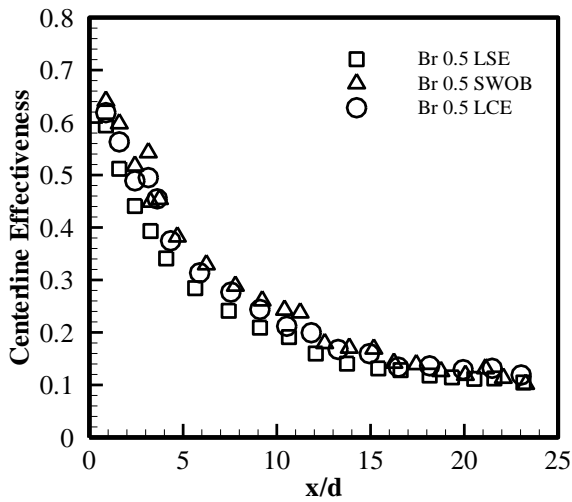
LCE

SWOB

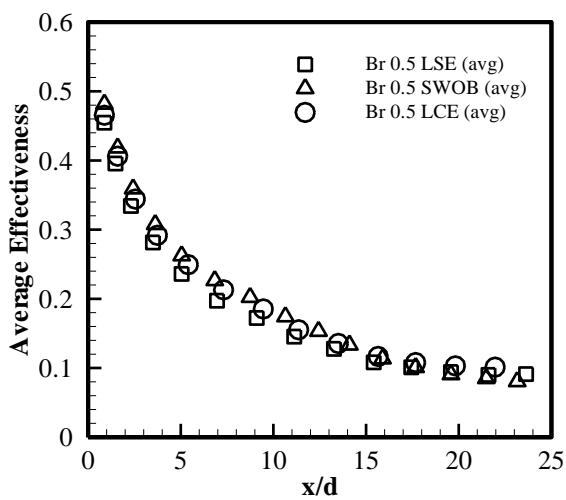
Figure 6, Sample surface images downstream different schemes at different blowing ratios (image#300)



a) Effectiveness Contours

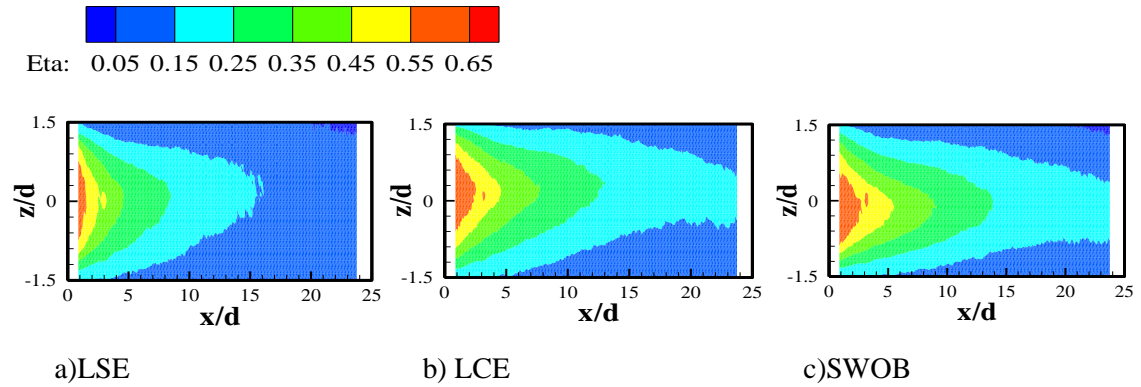


b) Centerline Effectiveness

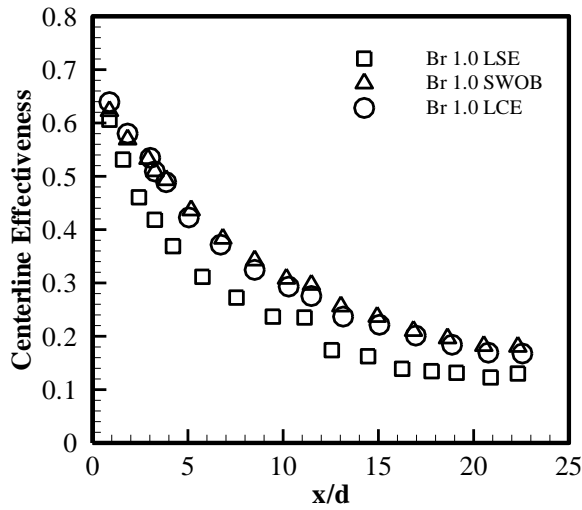


c) Spanwise-Averaged Effectiveness

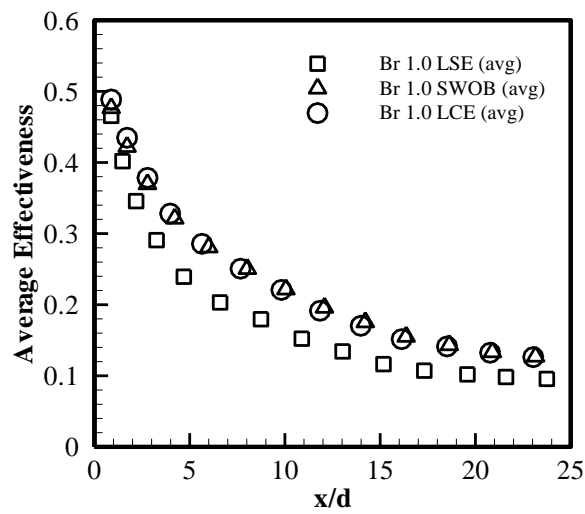
Figure 7, Effectiveness downstream different cases at $Br = 0.5$



a) Effectiveness Contours

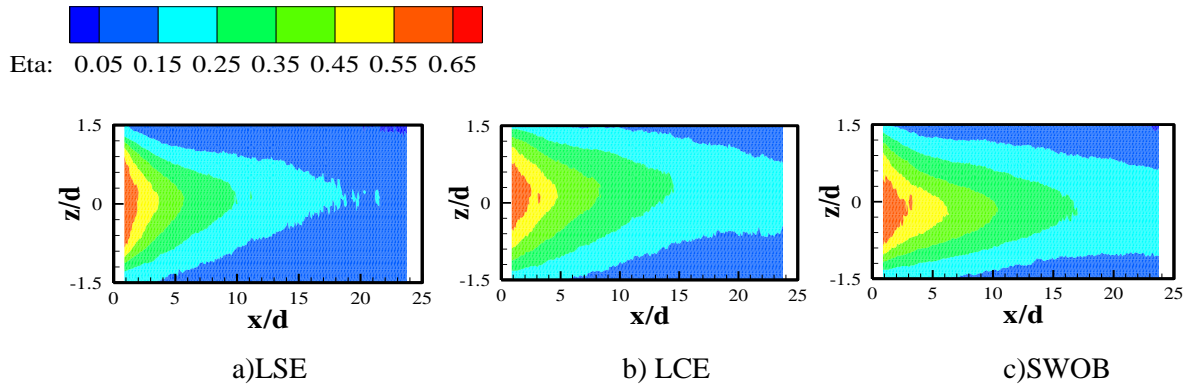


a) Centerline Effectiveness

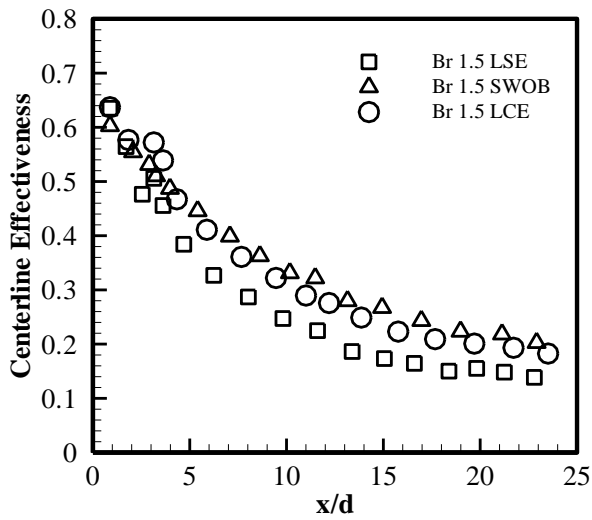


b) Spanwise-Averaged Effectiveness

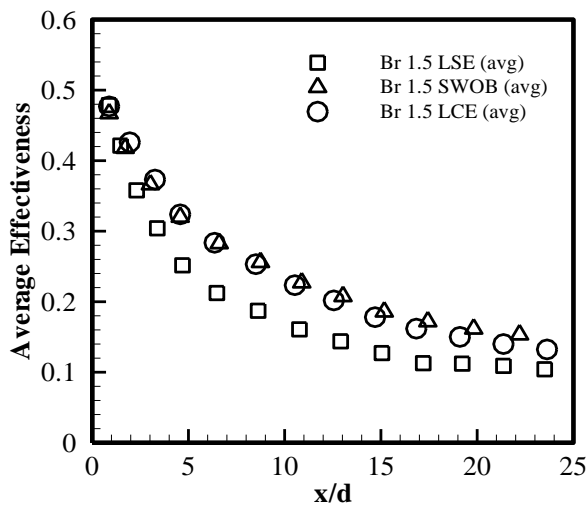
Figure 8, Effectiveness downstream different cases at $Br = 1.0$



a) Effectiveness Contours

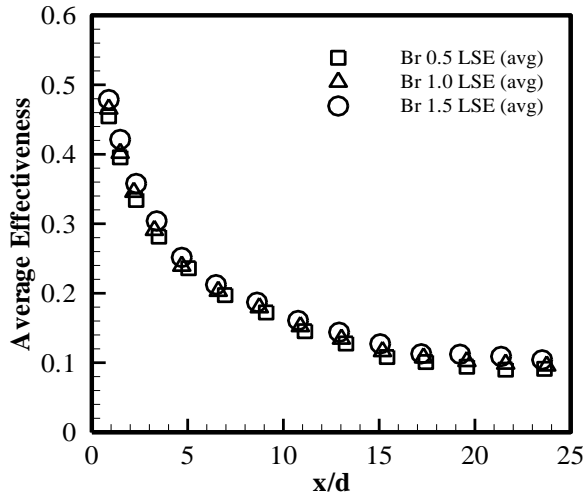


b) Centerline Effectiveness

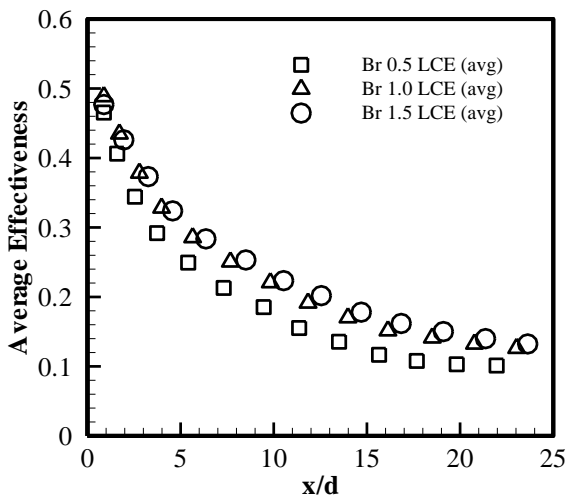


c) Spanwise-Averaged Effectiveness

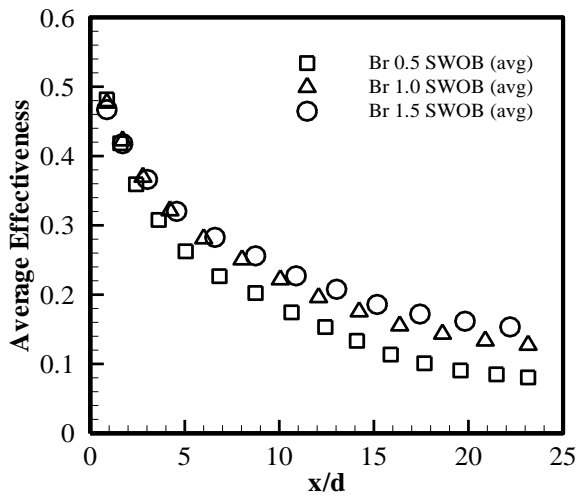
Figure 9, Effectiveness downstream different cases at $Br = 1.5$



a)



b)



c)

Figure 10, Blowing ratio effects on the spanwise-averaged effectiveness downstream different cases



HHOratio: 0.95 1 1.05 1.1 1.15 1.2 1.25 1.3

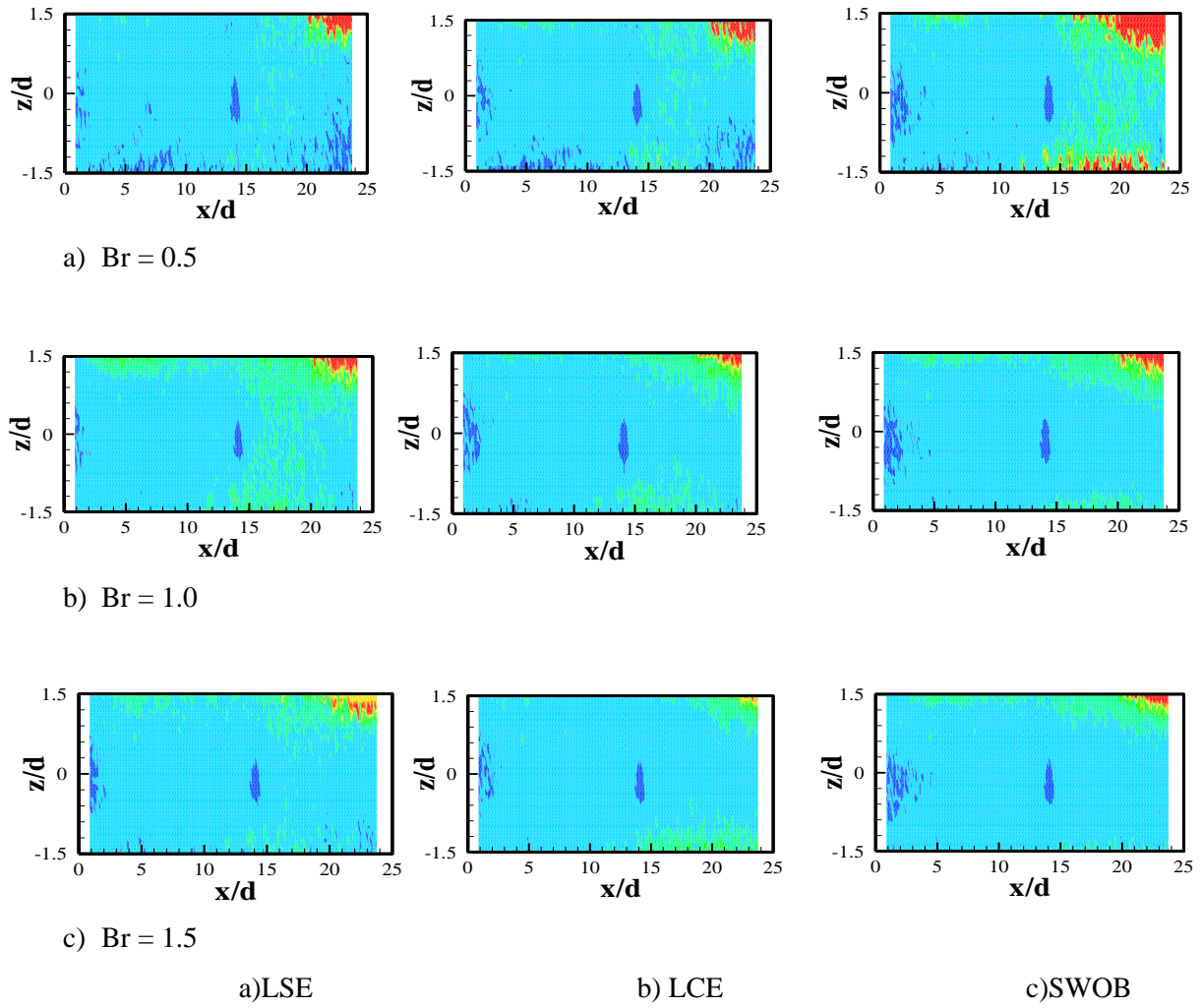


Figure 11, HTC ratio contours downstream different cases at different blowing ratios